Stochastic Particle Acceleration in Parallel Relativistic Shocks

Joni J. P. Virtanen
Tuorla Observatory, Väisäläntie 20, FI-21500 Piikkiö, FINLAND
Rami Vainio
Department of Physical Sciences, P.O. Box 64, FI-00014 University of Helsinki, FINLAND

We present results of test-particle simulations on both the first- and the second-order Fermi acceleration for relativistic parallel shock waves. Our studies suggest that the role of the second-order mechanism in the turbulent downstream of a relativistic shock may have been underestimated in the past, and that the stochastic mechanism may have significant effects on the form of the particle spectra and its time evolution. Figures are reproduced from Virtanen & Vainio 2005 [13] by the permission of the AAS.

1. INTRODUCTION

Particle acceleration in relativistic shocks is typically considered to be due to either the first- or the second-order Fermi acceleration (stochastic acceleration). The former of these acts at the shock front where charged particles gain energy by subsequently scattering on different sides of the shock front, whereas for the latter case the velocity difference between the scattering centers is provided by the turbulence alone. The first-order mechanism is well known to produce power-law particle energy spectrum $N(E) \propto E^{-\sigma}$ with spectral index σ depending on compression ratio r of the shock as $\sigma = (r+2)/(r-1)$ for nonrelativistic speeds [e.g., 1], and approaching to value $\sigma \approx 2.2$ as the speed increases to ultrarelativistic, almost regardless of the other shock conditions [e.g., 2–5].

However, problems arise with flatter spectra ($\sigma \lesssim 2$); although the first-order mechanism can produce harder spectra with $\sigma \to 1$ depending, for instance, on the injection model [6] or the scattering center compression ratio [e.g. 7–9], it is not able to produce spectral indices flatter than $\sigma = 1$.

Stochastic acceleration, on the other hand, has been known to be present in the turbulent downstream of shocks, but mostly because it works on much longer timescales than the almost instantaneous first-order mechanism [e.g., 10, 11] it has been been neglected for most of the cases (note, however, e.g. [12]). However, for non-thermal particle distributions radiating in astrophysical objects the bulk of radiation is emitted by the particles that have already left the shock front towards the downstream. Thus, the second order mechanism has, indeed, more time available to for acceleration than the first-order process. So while the neglecting of the stochastic process in calculation of the accelerated particle spectra right at the shock front could be justified, it is not possible to neglect its effect on the spectrum in shocks in general, especially when basically all of the astrophysical sources related to relativistic shocks, remain still spatially unresolved.

Here we study the possibility of the stochastic process to have visible effects on the particle energy spectrum in parallel relativistic shock waves in two different cases: (i) particles injected at the shock front and accelerated further by the first order mechanism and (ii) particles drawn from the heated (but not shock accelerated) particle population of the downstream region of the shock. We apply numerical Monte Carlo test-particle simulations and focus on shocks that, in addition to being parallel, have small-to-intermediate Alfvénic Mach number. Low Mach numbers for relativistic shocks could prevail in magnetically dominated jets that are lighter than their surroundings, e.g. in pair-plasma jets.

2. MODEL

The applied model, together with its numerical implementation, is described in detail in ref. [13], and here only the essential parts of the model are explained.

We use the shock rest frame as our basic coordinate system. In the case of parallel shock the flow direction – as well as the large scale magnetic field – is perpendicular to the shock normal in this frame. In this frame the shock lies at the origin, negative values of location x mean the upstream and positive values the downstream. The plasma frame, i.e. the frame where the bulk of the plasma is at rest, is moving with the local flow speed V with respect to the shock frame. Waves propagate at phase speed V_ϕ in the plasma frame in directions both parallel and antiparallel to the flow, so in the shock frame waves move at speed $(V + V_\phi)/(1 + VV_\phi/c^2)$ (c is the speed of light), and the frame moving at this speed (i.e. flowing with the waves) is called the wave frame or the rest frame of the scattering centers. If the scattering centers are taken to be fluctuations frozen-in to the plasma then the speed of the waves with respect to the underlying flow is $V_\phi = 0$ and the plasma frame is also the rest frame of the scattering centers. Here we assume the waves to be Alfvén waves, and the phase speed to be the Alfvén speed

$$v_{\rm A} = \frac{B_0 c}{\sqrt{4\pi h n + B_0^2}}, \qquad (1)$$

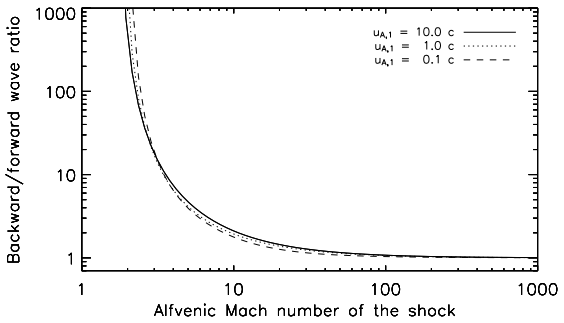

Figure 1: Ratio of the amplified wave intensities as function of Alfvénic Mach number for three proper Alfvén speeds. Here $q = 5/3$. [13]

where B_0 is the large scale magnetic field, and h and n the specific enthalpy and the number density, all in the local plasma frame.

We set the proper speed of the shock to be $u_1 \equiv \Gamma_1 V_1 = 10c$ (corresponding to shock speed $V_1 \approx 0.995\,c$), and model the shock transition with a very thin hyperbolic tangent profile [14] with thickness $W \approx \frac{1}{100}$th of the mean free path of an upstream particle. For this width the shock can still be considered almost step-like [5].

We model the downstream turbulence as a superposition of Alfén waves propagating parallel and anti-parallel to the plasma flow at constant speed. The turbulence spectrum has a power-law form with spectral index q for wavenumbers above some inverse correlation length k_0. For $k < k_0$ the wave intensity per logarithmic bandwidth is assumed to be equal to the background field intensity, i.e., $I(k) = B_0^2 k^{-1}$ for $k < k_0$. In this work we use two values for q: 2, producing rigidity independent mean free paths, and 5/3, being consistent with the Kolmogorov phenomenology of turbulence.

The downstream wave intensities can be calculated from known upstream parameters [e.g., 8, 9, 11], and regardless of the cross helicity of the upstream wave field (only parallel or anti-parallel waves, or both), there are always both wave modes present in the downstream region; in this work we assume the cross helicity to vanish in the upstream. The amplification of the waves at the shock depends on the strength of the magnetic field as well as on the form of the turbulence spectrum, as shown in Fig. 1 where the amplification of the different wave modes is shown as a function of (quasi-Newtonian) Alfvénic Mach number

$$M = u_{\mathrm{A},1}/u_1. \tag{2}$$

$$u_{\mathrm{A},1} = v_{\mathrm{A},1}/\sqrt{1-\beta_{\mathrm{A},1}^2}, \tag{3}$$

is the upstream Alfvén proper speed with $\beta_{\mathrm{A},1} = v_{\mathrm{A},1}/c$. The waves are seen to propagate predominantly backward for relatively low-Mach-number shocks; this is the case for both the relativistic [8] and the nonrelativistic [11] shocks. This enables the scattering center compression ratio r_k to grow larger than the gas compression ratio r and, thus, to cause significantly harder particle spectra compared to the predictions of theories relying on fluctuations frozen-in to plasma flow [8, 9]. As the Mach number increases, the downstream wave intensities approach equipartition at the ultra-relativistic limit.

Electrons scatter off the magnetic fluctuations resonantly. The scattering frequency of electrons with Lorentz factor γ is determined (see ref. [13] for details) by the intensity of waves at the resonant wavenumber

$$k_{\mathrm{res}} = \frac{\Omega_{\mathrm{e}}}{v} = \frac{\Omega_{\mathrm{e},0}}{c\sqrt{\gamma^2-1}}, \tag{4}$$

where $\Omega_{\mathrm{e}} = \frac{\Omega_{\mathrm{e},0}}{\gamma}$ is the relativistic electron gyrofrequency and $\Omega_{\mathrm{e},0} = \frac{eB}{m_e c}$ is its non-relativistic counterpart.

Scatterings are elastic in the wave frame and the existence of waves propagating in both directions at a given position, thus, leads to stochastic acceleration [15]. Since the spectrum of waves is harder below $k = k_0$, scattering at energies

$$\gamma > \gamma_0 \equiv \frac{\Omega_{\mathrm{e},0}}{k_0 c} \gg 1 \tag{5}$$

becomes less efficient. This suggests that the electron acceleration efficiency should decrease at $\gamma > \gamma_0$. Instead of trying to fix the value of k_0, we use a constant value $\gamma_0 = 10^6$, which is in agreement with observations of maximum Lorentz factor of electrons in some AGN jets [16].

In addition to scattering, the particles are also assumed to lose energy via the synchrotron emission.

3. RESULTS & DISCUSSION

Simulations were run separately for low, intermediate and high Alfvénic-Mach-number shocks ($M = 3$, $M = 10$, and $M = 1000$, respectively – see Fig. 1 for the corresponding wave intensity ratios), and for four cases of downstream turbulence; for turbulence spectral index $q = 2$ and $q = 5/3$ with downstream wave field calculated using wave transmission analysis described earlier, and with the downstream forward and backward waves being in equipartition. The proper speed of the shock is set to $u_1 = 10\,c$ in all simulations.

Some of the results (including all of the case of $M = 1000$ for which the effects were, expectedly, barely visible, and all those for which the downstream turbulence was calculated using the Alfvén wave transmission model) have been omitted from this paper due to limited space; all of them are, however, available at `http://www.astro.utu.fi/red/qshock.html`.

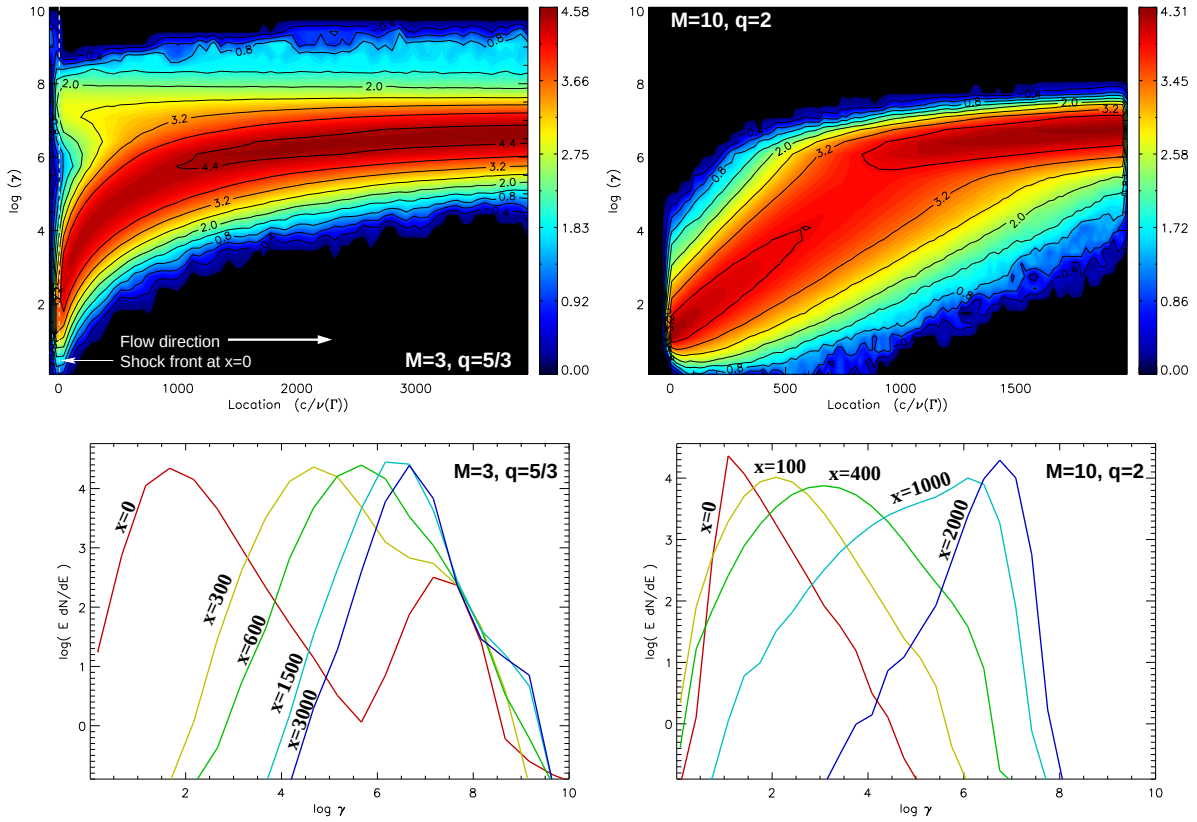

Figure 2: Steady-state energy distribution of shock-injected particles at different distances from the shock. Upper panels show contours of $\log(E\frac{dN}{dE})$ as function of energy and location, while the lower panels present the energy distributions as slices at certain locations in the downstream. On the left hand panel is a case with a shock with Alfvénic Mach number $M = 3$ and for turbulence corresponding to the Kolmogorov turbulence, and on the right panel the same for $M = 10$ and turbulence corresponding to that created by the particles themselves. Equipartition is assumed between forward and backward waves. [13].

3.1. Particles Injected at the Shock

In the first case we studied the effect of stochastic acceleration on particles that have been already accelerated at the shock. We injected the particles with relatively small initial energy into the simulation right behind the shock and allowed them to continue accelerating via the stochastic process. This kind of injection simulates the case of some already-energized downstream particles returning into the shock, but removes need of processing the time consuming bulk of non-accelerating thermal particles. The high-energy part of the particle energy distribution – which we are interested in in this study – is similar, regardless of the injection energy.

In the case of high Alfvénic Mach number ($M = 1000$, corresponding to magnetic field $B_0 \simeq 1.4$ mG in a hydrogen plasma and $\simeq 46\,\mu$G in a pair plasma) the contribution of the stochastic process to the energy distribution of the particles was, expectedly, very insignificant compared to that of the first-order acceleration at the shock. This was the case regardless of the applied turbulence properties, and because the wave intensities calculated from the Alfvén wave transmission analysis are very close to equipartition for high-Mach-number shock (see Fig. 1), the difference to the case of explicitely assumed equipartition was, as expected, minimal.

For shocks with Alfvénic Mach number sufficiently low ($M = 10$ and $M = 3$, corresponding to ≈ 0.1–0.5 G in a hydrogen plasma, and to ≈ 5–15 mG in a pair plasma) the effect was, on the contrary to the high-M case, very pronounced. The stochastic process began to re-accelerate particles immediately after the shock front, and the whole spectrum started to slowly shift to higher energies in all kinds of turbulence models studied. Two examples for the case assuming the downstream wave intensities to be in equipartition are shown in Fig. 2.

When comparing otherwise similar cases that differ only for the downstream cross helicity (i.e., whether the wave field is resulting from the wave transmission calculations [8] or an equipartition of parallel and anti-parallel waves is assumed), the calculated wave-

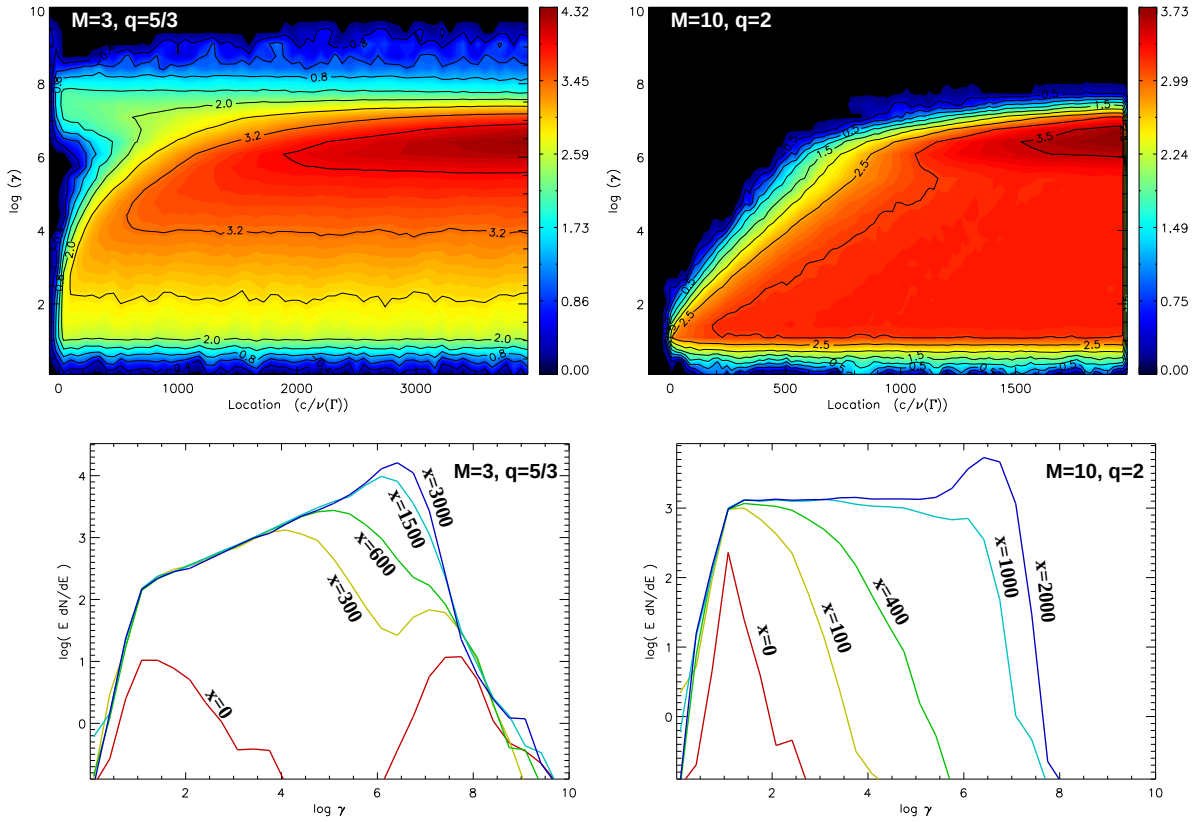

Figure 3: Same as Fig. 2 but for particles injected uniformly throughout the downstream region. [13].

transmission cases with more anti-parallel waves (see [8] and Fig.1) show stronger first-order acceleration, but weaker stochastic acceleration. This is because of the larger scattering center compression ratio in the wave-transmission case leading to more efficient first-order acceleration [8, and Virtanen & Vainio, in preparation] and, on the other hand, faster momentum diffusion rate in the equipartition case leading to more efficient stochastic acceleration.

3.2. Particles Injected Across the Downstream

Next we assumed that a constant injection mechanism exists throughout the downstream region – this mimics a case where turbulent fluctuations cascade to higher wavenumbers and inject a fraction of the thermal electrons to the stochastic acceleration process. We injected particles at a constant initial energy uniformly and isotropically within the whole downstream region. Examples of results are shown in Fig. 3 for parameters otherwise equal to those in Fig. 2.

The general behavior of the acceleration process is very similar for both injection methods: the piling up of the particles with $\gamma > \gamma_0$ is visible and the effect of the turbulence spectrum is the same. For the constant injection, however, particles begin to form a power-law plateau in the energy range between the injection energy and γ_0. The produced spectral index depends on the spectral index of the magnetic field fluctuations q as $\sigma = q - 1$ [13, 15]; for $q = 2$, the particle spectral index $\sigma \simeq 1$, and for $q = 5/3$, $\sigma \simeq 0.6$.

Also here the composition of the downstream wave field affects the resulting spectrum: in the case of downstream turbulence calculated using the wave transmission model the particle population immediately behind the shock front extends to slightly higher energies than in the equipartition case, but for the latter the stochastic acceleration is clearly quicker. The former effect is due to the scattering center compression ratio being larger for lower-M shocks, while the latter is due to larger velocity differences in the equipartition wave field.

3.3. "Re-acceleration of Re-accelerated Particles"

The prolonging of the mean free path of particles with $\gamma > \gamma_0$ (or $k_{\rm res} < k_0$) has, in addition to the drop of the stochastic acceleration efficiency, another

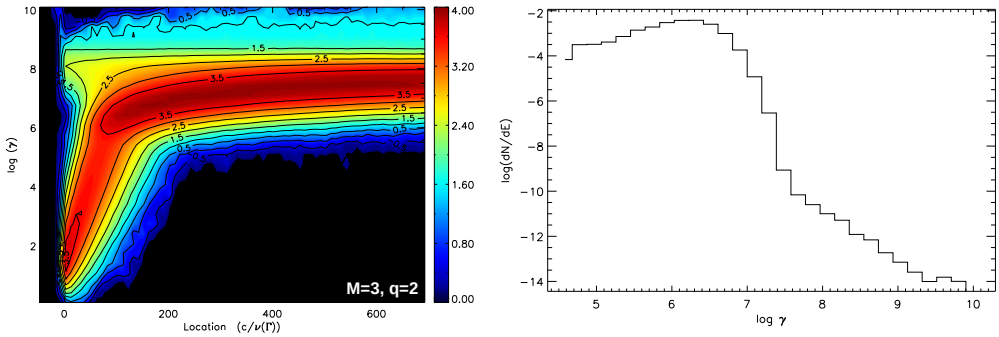

Figure 4: Stochastically accelerated particles return to the shock and get re-accelerated by the first-order process. On the right the particles are gathered at downstream free-escape boundary. [13]

interesting feature: particles that are already energized first in the shock by the first-order mechanism and then in the downstream by the second-order acceleration, become able to return back to the shock and get "re-injected" into the first-order acceleration process. Injection energies for this second injection are very high, or course, so particles get accelerated to ultra-high energies; this is seen as a distortion of the high-energy part of the left-hand contour panels in Figs. 2 and 3, and especially clear in Fig.4, where the low Mach number $M = 3$ and turbulence corresponding to $q = 2$, both favorable for fast stochastic acceleration, allow particles to be accelerated to energies of the order of γ_0 while still being sufficiently close to the shock front in order to being able to return to the first-order acceleration process. As a result, a clearly visible high-energy (quasi) power-law is seen in the upper part of the contour as well in the energy spectrum collected at the downstream border.

3.4. Combination of Injection Mechanisms

We also investigated what kind of particle energy spectra the two injection schemes – one operating at the shock, and another operating uniformly throughout the downstream region – are able to create. Fig. 5 gives an example of combination of these. In simulations these two acceleration cases were mostly kept separate for the sake of simplicity, but there should be no reason to assume the separation be present also in nature. Also the relative amounts of shock- and downstream-injected particles are not fixed by our model, but instead considered a parameter.

4. CONCLUSIONS

We have studied stochastic particle acceleration in the downstream region of a relativistic parallel shock.

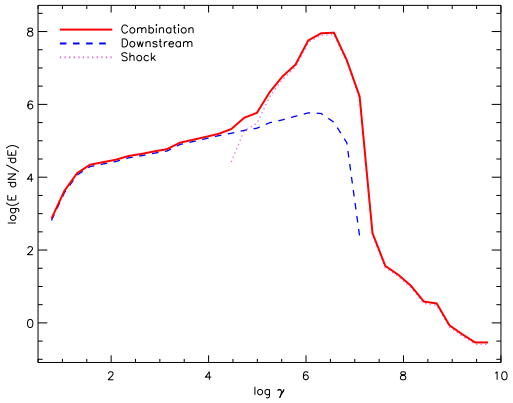

Figure 5: Example of a combination (solid line) energy spectra of particles injected to the acceleration process at the shock (dotted) and throughout the downstream region (dashed). (Model parameters are $q = 5/3$ and $M = 10$.) The particles are collected at the downstream free escape boundary, $\sim 4 \times 10^{12}$ cm away from the shock, and the number of the particles injected at the shock is larger than the number of uniformly injected particles by a factor of 100. [13]

Applying the wave transmission calculations of [8] and assuming the cross helicity to vanish in the upstream, we have modeled the turbulence of the downstream region as a superposition of Alfvén waves propagating parallel and anti-parallel to the plasma flow. Using a kinetic Monte Carlo simulation we have modeled the second-order Fermi acceleration of electrons in the shock environment, and considered cases of acceleration of downstream-injected particles, as well as that of particles injected at the shock. We have shown that the stochastic acceleration can, indeed, have remarkable effects in both cases. This result is even more pronounced if the two downstream Alfvén wave fields are assumed to be in equipartition.

The behavior of the particle energy distribution in

the stochastic process depends heavily on the strength of the background magnetic field; in the cases of weak magnetic field and large quasi-Newtonian Alfvénic Mach number the effects of stochastic acceleration are faded out by the much stronger first order acceleration. Also the magnetic field turbulence spectrum affects the acceleration efficiency: for Kolmogorov turbulence with $q = 5/3$ the spatial scales are up to an order of magnitude shorter than in the case of $q = 2$ turbulence. Although the spatial scales in simulations presented here are enormous compared to those associated with shock acceleration (the first-order process in the immediate vicinity of the shock front), in case of blazars and other active galactic nuclei the scales are still orders of magnitude too small to be resolved even in the VLBI pictures – regardless of the turbulence and used magnetic field strength. Also the acceleration time scales are short: the time required to shift the whole spectrum from the initial energy range to $\gamma_{\rm bulk} \gtrsim 10^6$ ranged from 10 to 50 minutes in the $M = 10$ case, and for $M = 3$ the times were $\lesssim 1$ minute, as measured in the shock frame.

In the cases where the stochastic acceleration was quick enough for particles to reach the γ_0 energy while being still sufficiently close to the shock in order to be able to make their way back to the upstream region due to their prolonged mean free path, the first-order mechanism was able to re-accelerate the returning high-energy particles to even higher energies. This led to forming of a new (quasi-)power-law at energies $\gamma \gtrsim 10^7$ in some cases.

One notable feature of the present model is that in the case of a uniform injection process in the downstream region, power-law spectra with high and low energy cut-offs are formed. Depending on the turbulence, particle energy spectra have power-law spectral indices of 0.5–1 with lower and higher energy cut-offs at $\gamma_1 \approx 10^1 \simeq \gamma_{\rm injection}$ and $\gamma_2 \sim 10^6 = \gamma_0$, respectively. These particles would produce synchrotron spectra with photon spectral indices $-0.5 < \alpha < 0$ in the GHz–THz regime for various initial parameters. These properties are quite similar to those of flat-spectrum sources, for which typical spectra with $\alpha \gtrsim -0.5$ in the GHz region and flare spectra with $\alpha \approx -0.2$ in the optically thin region of the spectrum are seen; see e.g. [17] and references therein.

To conclude, the main results of this study are:

- Stochastic acceleration can be a very efficient mechanism in the downstream region of parallel relativistic shocks, provided that the magnetic field strength is large enough in order to make the Alfvénic Mach number approach the critical Mach number ($M_{\rm c} = \sqrt{r}$) of the shock, i.e., to increase the downstream Alfvén speed enough to allow for sufficient difference in speeds of parallel and anti-parallel Alfvén waves required for rapid stochastic acceleration.

- In the case of a continuous injection mechanism in the downstream region particle energy distributions with hard spectral indices can be formed between the injection energy and γ_0. The accelerated particle populations could produce synchrotron spectra very similar to those of flat spectrum sources.

- The interplay between the first- and second-order Fermi acceleration at relativistic shocks can produce a variety of spectral forms not limited to single power laws.

Remark: We wand to emphasize that these simulations are based on the test-particle approximation, i.e., the effects of the particles on the turbulent wave spectrum and on the shock structure are neglected. Including these effects in a self-consistent manner may lead to notable effects on the resulting spectrum, see e.g. [18]. Including these effects to our model is, however, beyond of the scope of the present simulations.

References

[1] Drury L. O'C. 1983, Rep. Prog. Phys. 46, 973
[2] Kirk J. G, Guthmann A. W., Gallant Y. A. & Achterberg A. 2000, ApJ 542, 235
[3] Achterberg A., Gallant Y. A., Kirk J. G. & Guthmann A.W. 2001, MNRAS 328, 393
[4] Lemoine M. & Pelletier G. 2003, ApJ 589, L73
[5] Virtanen J. J. P. & Vainio R. 2003, in ASP Conf. Proc. 299, High Energy Blazar Astronomy, ed. Takalo, L. O., & Valtaoja, E., 143
[6] Virtanen J. J. P. & Vainio R. 2003, Proc. Internat. Cosmic Ray Conf., OG 1.4, 2023
[7] Ellison D. C., Jones F. C. & Reynolds S. P. 1990, ApJ 360, 702
[8] Vainio R., Virtanen J. J. P. & Schlickeiser R. 2003, A&A 409, 821
[9] Vainio R., Virtanen J. J. P. & Schlickeiser R. 2005, A&A 431, 7
[10] Campeanu A. & Schlickeiser R. 1992, A&A 263, 413
[11] Vainio R. & Schlickeiser R. 1998, A&A 331, 793
[12] Ostrowski M. & Schlickeiser R. 1993, A&A 268, 812
[13] Virtanen J. J. P. & Vainio R. 2005, ApJ 621, 313
[14] Schneider P. & Kirk J. G. 1989, A&A 217, 344
[15] Schlickeiser R. 1989, ApJ 336, 243
[16] Meisenheimer K., Röser H.-J. & Schlötelburg M. 1996, A&A 307, 61
[17] Valtaoja E., et al. 1988, A&A 203, 1
[18] Vainio R. 2001, Proc. Internat. Cosmic Ray Conf., 6, 2054